Mem. S.A.It. Suppl. Vol. 4, 61

Memorie della
Supplementi

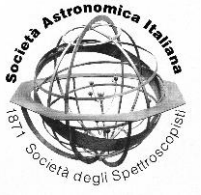

Grid-adaptive computations for magnetized astrophysical plasmas

R. Keppens[1], J. Bergmans[2], and H. Baty[3]

[1] FOM Institute for Plasma Physics Rijnhuizen, P.O. Box 1207, 3430 BE Nieuwegein, The Netherlands e-mail: keppens@rijnh.nl
[2] Astronomical Institute, Utrecht University, P.O. Box 80000, 3508 TA Utrecht, The Netherlands
[3] Observatoire Astronomique, 11 Rue de l'université, 67000 Strasbourg, France

Abstract. Magnetized plasma dynamics is of central importance in a great variety of astrophysical phenomena, and poses particular challenges to computational studies. We review the development history of the Versatile Advection Code, a software package designed for simulating magnetohydrodynamic processes, and discuss its current extension to grid-adaptive simulations. Adaptive mesh refinement is essential to capture plasma flow details which play a role in long-term dynamical evolutions. A specific example is given for magnetized shear flow layers, where large-scale coalescence effects go hand-in-hand with small-scale magnetic field reconnections. Grid-adaptivity is also a prerequisite for accurately handling relativistic hydro- and magnetohydrodynamic flow problems. Examples of the latter are presented with an outlook to ongoing astrophysically relevant applications.

Key words. MHD – AMR – relativistic flows

1. Magnetized Plasma-Astrophysics

It is commonly stated that the vast majority of visible matter in our universe is in the plasma state, where free electrons and ionized atoms/molecules form a macroscopically neutral substance. Since charged particles have associated longe-range electromagnetic forces, they exhibit collective effects which make the plasma state of matter quite distinct from ordinary fluid behavior. Perhaps the best known example of intricate plasma behavior is provided by our own Sun. There, the dynamics of the plasma constituting our Sun is generating the Sun's internal magnetic field, which in turn shapes the Sun's corona visible at solar eclipses. It is grossly understood how both large-scale and small-scale plasma flows in the solar interior contribute to a cyclic waxing and waning of the solar magnetic field through a dynamo action. The magnetic topology of the solar corona thereby changes from predominantly dipolar during the solar minimum, to a collection of loops, arcades, and continuously rearranging magnetic complexes at the time of solar maximum. Especially in this most active magnetic phase, the solar corona is a prime example of magnetized plasma dynamics, with eruptive events up to scales and en-

Send offprint requests to: R. Keppens
Correspondence to: P.O. Box 1207, 3430 BE Nieuwegein

ergies sufficient to influence the Earth's magnetosphere. A lot of research effort is currently en route towards predictive computations for the most violent of these so-called 'Space Weather' events (De Sterck & Poedts 1999; Mikić et al. 1999; Powell et al. 1999; Odstrčil & Pizzo 1999). A common approach is to simulate the coronal dynamics as governed by a set of conservation laws for the macroscopic behavior of a perfectly conducting plasma: the magnetohydrodynamic (MHD) description. Since the MHD equations have the property to be independent of the length, time, and mass scale, they form an ideal starting point to numerically model not only coronal, but general magnetized plasma-astrophysical phenomena.

2. Magnetohydrodynamics

The ideal MHD description offers a continuum, single fluid viewpoint of a plasma in terms of the plasma density ρ, the velocity vector $\mathbf{v}$, the pressure p, and the magnetic field $\mathbf{B}$. The 8 equations describe conservation of mass, momentum, energy, and magnetic flux, written as

$$\frac{\partial \rho}{\partial t} + \nabla \cdot (\mathbf{v}\,\rho) = S_\rho \quad (1)$$

$$\frac{\partial \rho \mathbf{v}}{\partial t} + \nabla \cdot (\mathbf{v}\,\rho\mathbf{v} - \mathbf{B}\,\mathbf{B}) + \nabla p_{\rm total} = \mathbf{S}_{\rho v} \quad (2)$$

$$\frac{\partial e}{\partial t} + \nabla \cdot (\mathbf{v}\,e + \mathbf{v}\,p_{\rm total} - \mathbf{B}\,\mathbf{B}\cdot\mathbf{v}) = S_e \quad (3)$$

$$\frac{\partial \mathbf{B}}{\partial t} + \nabla \cdot (\mathbf{v}\,\mathbf{B} - \mathbf{B}\,\mathbf{v}) = \mathbf{S}_B. \quad (4)$$

These are expressed in the conservative variables density ρ, momentum density $\rho\mathbf{v}$, total energy density e, and magnetic field $\mathbf{B}$, with all additional sources and sinks collected in the source terms S_ρ, $\mathbf{S}_{\rho v}$, S_e and $\mathbf{S}_B$. In these equations, the total kinetic and magnetic pressure is written as

$$p_{\rm total} = (\gamma - 1)\left(e - \frac{1}{2}\rho\mathbf{v}^2 - \frac{1}{2}\mathbf{B}^2\right) + \frac{1}{2}\mathbf{B}^2, \quad (5)$$

for an ideal gas with adiabatic index γ. An additional restriction is posed by one of Maxwell's equations, namely

$$\nabla \cdot \mathbf{B} = 0, \quad (6)$$

so that magnetic field lines, everywhere tangent to the local magnetic field vector, have no beginning or end. The MHD equations written above are valid for non-relativistic plasma flows, but a special relativistic variant can be formulated as well. The relativistic MHD equations describe magnetized plasma flows at near light speed, and again express particle conservation, conservation of the momentum-energy tensor, and the unchanged induction equation (4) for the magnetic field. In both the classical and the relativistic MHD equations, the gas dynamical limit emerges from setting $\mathbf{B} = 0$.

3. Versatile Advection Code

The Versatile Advection Code (VAC), initiated by Tóth (1996), is a software package designed for integrating numerically a set of (near-) conservation laws in any dimensionality. In particular, the set of MHD equations (1)–(4) augmented with the constraint (6), has been used as model equations in a fair variety of solar and astrophysical applications. These include dynamics in the solar corona and heliosphere, ranging from coronal loop simulations where footpoint motions cause waves to propagate and dissipate their energy at higher coronal altitudes (Beliën et al. 1999), to simulations of the solar wind and forced coronal mass ejections (Keppens & Goedbloed 2000), to heliospheric perturbations developing in-situ as a result of MHD instabilities (Zaliznyak et al. 2003). Recent astrophysical simulations have focused on magnetized jets associated with young forming stars or with more exotic objects like black holes and neutron stars. They elucidated how jets are launched from magnetized accretion disks (Casse & Keppens 2002, 2004), and how interacting MHD instabilities may play a role in maintaining jet coherency (Baty & Keppens 2002).

The VAC code is one of the main achievements in an interdisciplinary effort on parallel computational magneto-fluid dynamics, where 8 teams within the Netherlands collaborated in

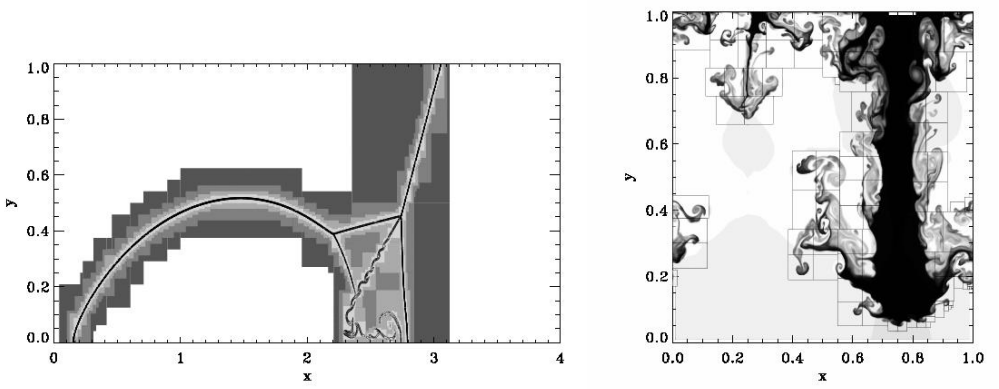

Fig. 1. *Left panel:* A 2D hydro simulation of a reflected Mach 10 shock, computed with 5 grid levels to reach 3072×768 grid accuracy. A Schlieren plot of the density structure is shown at $t = 0.2$. *Right panel:* Heavy mixing into lighter matter in a Rayleigh-Taylor unstable configuration. Logarithm of the density at time $t = 1.9$ from a 5 grid level AMR simulation.

a Priority Program of the national Scientific Research Organization (NWO). The code is designed in a modular fashion, where the set of equations to solve and the particular temporal or spatial discretization method to integrate them is implemented in a rather interchangeable manner. Specifically for the MHD equations, VAC offers a choice of five explicit, shock-capturing second order schemes (Tóth & Odstrčil 1996), as well as many options for handling the solenoidal constraint on **B** (Tóth 2000). The code always employs cell-centered quantities representing volume averages on a structured grid. The dimensionality of the problem can be set prior to compilation of the code, since the source is written in a dimension-independent fashion where its Fortran 90 style is augmented with the Loop Annotation SYntax (LASY, Tóth (1997)). Originally, data parallelism was achieved by means of High Performance Fortran (Keppens & Tóth 2000), but more recent applications make use of automated OpenMP parallelism, which demonstrated linear scaling properties up to few tens of processors (Keppens et al. 2002). An MPI-based implementation will be released during 2004 (Tóth G., private communication), making VAC suitable for fully distributed memory parallel execution.

4. VAC and Adaptive Mesh Refinement: AMRVAC

In many gas- and magnetofluid computations of astrophysical interest, a hierarchy of spatial scales need to be resolved simultaneously for extended time periods. This justifies the need for parallel computing, allowing high resolution studies on otherwise fixed grids. However, with the notable exception of fully developed turbulence simulations, there is typically no need for a uniformly high grid spacing at all times. It suffices to track and resolve the small, localized structures (shocks, contact discontinuities, strong shear layers) at a high resolution, combined with coarser grids to capture the more global, smooth flow features. A version of VAC has now been extended with a dynamic regridding methodology known as Adaptive Mesh Refinement (AMR, see Berger & Colella (1989)), to efficiently compute classical, as well as relativistic (Bergmans et al. 2004) hydro- and MHD problems. The AMRVAC (Keppens et al. 2002; Nool & Keppens 2002; Keppens et al. 2003) software is again easily configured to any dimensionality, and offers choices in conservative, high resolution spatial discretizations combined with explicit time integration. The grid hierarchy is one of properly nested 'rectangular' patches,

Table 1. Selected 3D simulations using up to $l_{\max}$ AMR grid levels, timings in seconds and corresponding efficiency reached. The effective resolution and time interval is listed at left.

problem	method	$l_{\max}$	timing	eff.
3D Advection	TVDLF	1	172197	–
$320^3 \times [0,1]$		3	8653	19.90
3D MHD	TVDMU	1	218650	–
Rayleigh-Taylor	TVDLF-MU (1-1)	2	46659	4.69
$80 \times 160 \times 80 \times [0,1]$	TVDLF-MU (2-1)	3	40726	5 .37
3D MHD *Implosion*	TVDLF	1	39437	–
$240^3 \times [0,0.4]$		3	4733	8.3

where 'rectangle' is to be interpreted according to dimensionality. On each grid level, many individual, different-sized but non-overlapping grid patches are managed, which track flow features in a manner dictated by the ensuing dynamics. OpenMP parallelism can be exploited (Keppens & Tóth 2002), where the dynamically scheduled threads execute the time integration of the multiple grids on a certain AMR grid level in parallel.

Figure 1 shows two 2D hydrodynamical applications, where AMR capabilities are nearly indispensible. At left, an example taken from Nool & Keppens (2002), the well-known 2D reflected shock problem introduced by Woodward & Colella (1984) is computed at an effective resolution of 3072×768. A Schlieren plot of the density is shown, together with the 5 level grid structure used in the simulation. Notice how the grids nicely trace the various shock and contact discontinuity features. Moreover, at this resolution one starts to see the small-scale Kelvin-Helmholtz type instabilities along the jet head behind the principle Mach stem and along the contact discontinuity.

At right, a snapshot from a Rayleigh-Taylor unstable configuration is shown (taken from Keppens et al. (2003)), where the heavy (dark) material mixes into the light material underneath it under the influence of gravity. As the smaller length scales are more unstable, this mixing process quite naturally develops flow features at all scales. The effective resolution reached is 800×800 and exploited 5 grid levels. Only the highest grid level contours are indicated on this plot.

4.1. Efficiency considerations

Keppens et al. (2003) discussed in detail how efficient AMR simulations can be, for a variety of 1D, 2D and 3D hydro- and MHD problems. Specifically, 2D hydro simulations like those shown in Fig. 1 easily outperform corresponding high resolution, static grid runs by factors of 10 to 20 in execution time. The solution accuracy is thereby not sacrificed. Table 1 summarizes specific timings for selected 3D problems, whose setup is discussed in Keppens et al. (2003). A 3D pure advection problem at effective resolution 320^3 was shown to compute twenty times faster when comparing a static 320^3 run with an AMR run with only three grid levels. The two listed 3D MHD simulations, a 3D MHD realisation of a Rayleigh-Taylor problem as in Fig. 1 and a 3D implosion simulation, were found to reach the optimal efficiency possible. For the Rayleigh-Taylor test case, a beneficial strategy is to exploit a different spatial discretization method on the various AMR grid levels. For the 3D implosion test, the 'optimal efficiency' meant that the execution time was reduced by a factor 8 when allowing for 3 grid levels. This particular timing compares wall clock times for OpenMP parallel execution on 16 processors of the SGI Origin 3800, for both the domain-decomposed static grid case as well as the AMR run. The eightfold decrease is optimal when taking into account the domain coverage of the second and

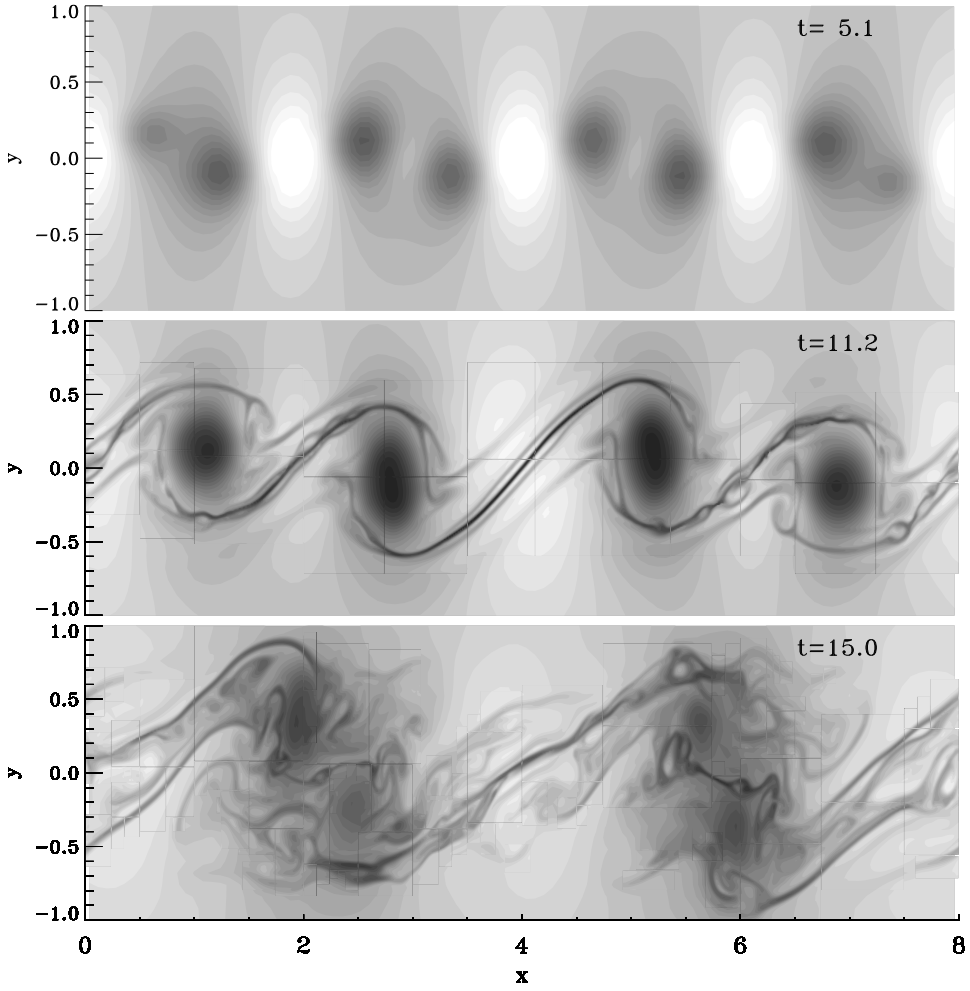

Fig. 2. Three density snapshots in the evolution of a single shear flow layer with Mach number $M = 1$ and Alfvén Mach number $M_A = 30$. Notice the pairing/merging of vortices to form large-scale structures, and the sudden appearance of (magnetic) islands at $t = 11$ leading to a turbulent disruption.

third grid levels, and further advantages of the AMR simulation are in reduced memory requirements as well as significant I/O reduction. The use of more grid levels, in combination with a sufficient resolution at the lowest level, is expected to reach much higher efficiencies than those of Table 1.

4.2. Coalescence in flow shear layers

A recent application of AMRVAC is by Baty et al. (2003), where 2D MHD simulations of a single shear flow layer are presented. A simple velocity profile $v_x = 0.5\,V \tanh 20y$ on a 2D grid $[0, L_x] \times [-L_y, +L_y]$ and otherwise uniform thermodynamic properties and flow-aligned magnetic field is characterized by its Mach number $M = V/c_s$, with sound

speed $c_s = \sqrt{\gamma p/\rho}$, and Alfvén Mach number $M_A = V/(B/\sqrt{\rho})$. Initiated by a small random vertical velocity perturbation, a transonic shear layer with $M = 1$ and a very weak initial magnetic field corresponding to $M_A = 30$ is Kelvin-Helmholtz (KH) unstable and a vortical flow pattern develops. Its streamwise extension is roughly of order unity under the chosen parameter settings, which corresponds to the horizontal wavelength $\lambda_{x,m}$ of the most unstable KH mode. When simulating extended segments of this single shear layer configuration, spanning multiple wavelengths $\lambda_{x,m}$, unstable subharmonic modes can grow up as well, and a continuous process of pairing/merging vortices was identified. In Fig. 2, snapshots of the initially uniform density variation for $L_x = 8$ show how at time $t = 5$ eight vortices have formed causing alternate regions of compressed and rarified plasma. Already at this time, pairing is evident which is continued throughout the further evolution. At time $t = 11$ only 4 vortices remain, and the final time shown contains two large-scale structures. For this value of the Alfvén Mach number, it was shown that the initially weak magnetic field gets amplified locally in strands at the vortex perimeter. It survives multiple vortex mergers without disruptive effect, and ultimately meets in strongly localized current sheets where sudden tearing-type reconnection events start. In the frame at $t = 11$, these are seen in the density as small-scale density features at the vortex periphery. A rapid transition to a turbulent MHD regime then occurs. This kind of magnetofluid processes, where a trend to large-scale coalescence is occuring simultaneously with localized instabilities and small-scale reconnections, is ideally suited for grid-adaptive computation. Since shear flow layers are present in nearly all solar and astrophysical plasma configurations, this highly idealized model problem demonstrates the need for AMR capabilities in more realistic applications.

4.3. Relativistic astrophysical flows

As relativistic speeds are observed or inferred in association with a variety of astrophysical sources, e.g. Active Galactic Nuclei, relativistic flow solvers are needed. To confirm the need for AMR in relativistic simulations, an example of a 1D spherical explosion taken from Bergmans et al. (2004) is shown in Fig. 3.

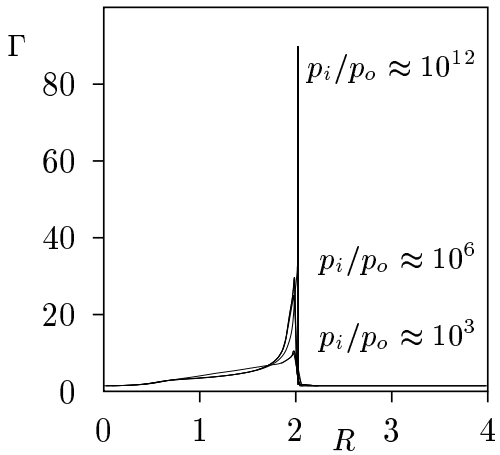

Fig. 3. A spherical explosion for different initial energies: ultra-relativistic speeds with strong and narrow shock structures call for AMR simulations.

The problem setup is a straightforward relativistic hydrodynamic 'shock tube' in spherical symmetry. Within a radius $R = 0.1$, the pressure p_i is a constant factor above the exterior pressure $p_o = 0.001$, and the plasma is static with unit density initially. The figure shows the Lorentz factor at time 1.9, for three different initial pressure ratios ranging from 10^3 to 10^{12}. For more energetic blast wave simulations, the Lorentz factor easily reaches order 100, and the Lorentz contraction causes the dense shell of swept up matter to become extremely narrow. Therefore, this simulation exploited 4 grid levels, a base grid of 1000 cells, with a refinement factor of 4 between successive levels: an effective resolution of 256000.

A much more demanding computation is illustrated in Fig. 4, which shows a snapshot of a 2.5D magnetized relativistic jet simulation exploiting mesh refinement. This calculation is performed with the new RMHD module of AMRVAC (Bergmans et al. 2004) on a base grid of 100×200 cells with three additional levels of refinement, resulting in an ef-

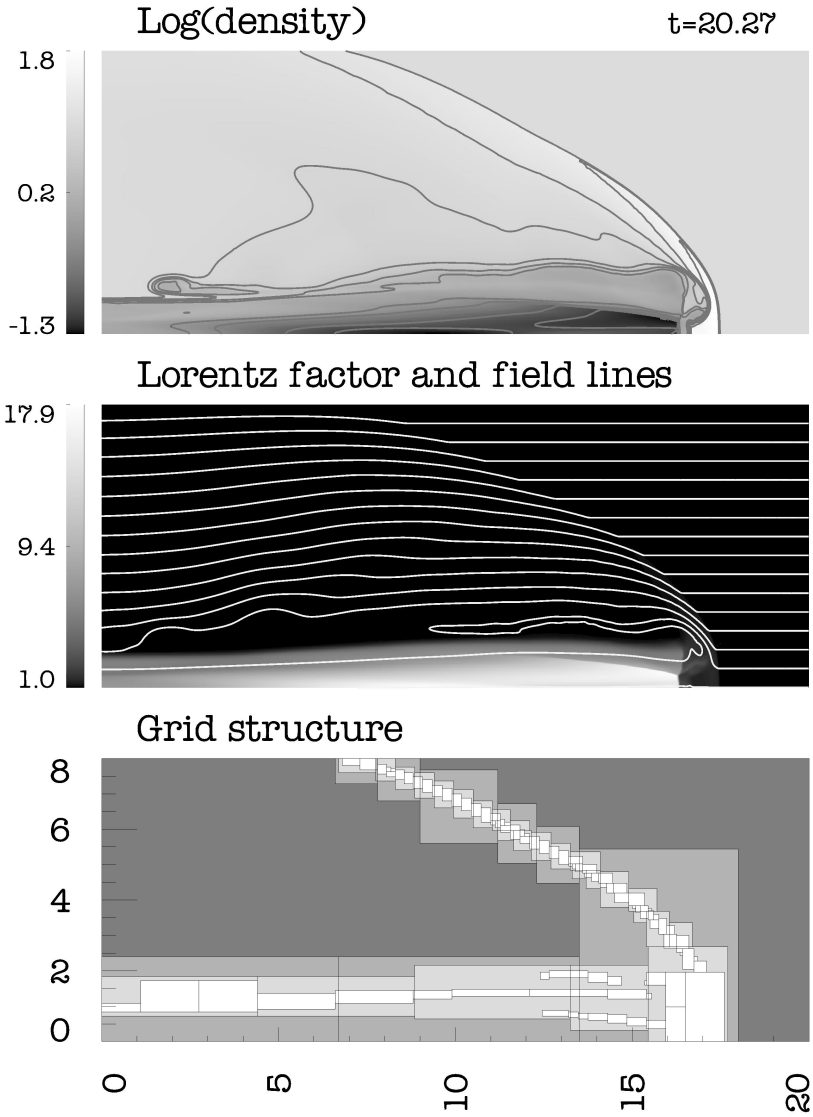

Fig. 4. A magnetized relativistic jet, injected at left at $\Gamma = 7$, with a helical internal magnetic field structure. The symmetry axis is the horizontal z-axis.

fective resolution of 800×1600. The jet is injected with a velocity $v_z \approx 0.99$ (corresponding to a Lorentz factor of about 7) into a two-dimensional axisymmetric domain $0 \le r \le 8$, $0 \le z \le 20$ with background density $\rho_e = 10$, pressure $p_e = 1.0$, and a parallel magnetic field $B_z = 0.1$. The jet radius at $z = 0$ is $R_j = 1$ and the density of the injected matter is $\rho_j = 1$. The jet has an additional toriodal magnetic field component given by

$$B_\phi = \begin{cases} b_m(r/R_m) & \text{for } r \le R_m, \\ b_m(R_m/r) & \text{for } R_m < r \le R_j, \\ 0 & \text{for } r > R_j, \end{cases} \qquad (7)$$

where $b_m = 1.0$ and $R_m = 0.37$. The transversal pressure profile is such that the jet is in hydromagnetic equilibrium at $z = 0$, both internally and with its surroundings. Shown in Fig. 4 is the grid structure, as well as the poloidal field structure, Lorentz factor, and density variation at $t \simeq 20$. Future work will address the detailed flow dynamics of such relativistic jets, and compare magnetized cases with pure relativistic hydro jets.

5. Outlook

Adaptive techniques, originally developed for compressible gas dynamics simulations, are gaining increased usage in magnetized plasma computations. Magnetofluid behavior typically involves both large and small scale effects which can only efficiently be simulated by using some form of automated regridding. We presented examples of both classical and relativistic MHD applications, where the benefits of adaptive mesh refinement are obvious. Especially in the study of magnetized plasma jets, the advent of general-purpose codes that incorporate grid-adaptation will allow to do thorough parameter studies. These can then be validated against actual laboratory experiments, and/or advance our understanding of classical up to ultra-relativistic astrophysical jet behavior.

Acknowledgements. This work was supported in part by the European Community's Human Potential Programme under contract HPRN-CT-2000-00153, PLATON, and by the NWO Computational Science project 'Rapid Changes in Complex Flows', coordinated by Prof. J.P. Goedbloed.

References

Baty, H., & Keppens, R. 2002, ApJ 580, 800
Baty, H., Keppens, R., Comte, P. 2003, Phys. of Plasmas 10(12), 4661
Beliën, A.J.C., Martens, P.C.H., Keppens, R. 1999, ApJ 526, 478
Berger, M.J. & Colella, P. 1989, J. Comput. Phys. 82, 64
Bergmans, J., Keppens, R., van Odyck, D.E.A., Achterberg, A. 2004, Lect. Notes in Comp. Science and Engineering, Proceedings of Chicago Workshop on Adaptive Mesh Refinement Methods (September 3-5, 2003), in press
Casse, F., & Keppens, R. 2002, ApJ 581, 988
Casse, F., & Keppens, R. 2004, ApJ 601, January 2004 issue
De Sterck, H. & Poedts, S. 1999, J. Geophys. Res. 104, 22401
Keppens, R. & Goedbloed, J.P. 2000, ApJ 530, 1036
Keppens, R., Nool, M., Goedbloed, J.P. 2002, in Parallel Computational Fluid Dynamics – Practice and Theory, eds. P. Wilders et al. (Elsevier Science B.V.) 215
Keppens, R., Nool, M., Tóth, G., Goedbloed, J.P. 2003, Comput. Physics Comm. 153, 317
Keppens, R., & Tóth, G. 2000, Parallel Computing 26, 705
Keppens, R., & Tóth, G. 2002, in Proceedings ICCS 2002, eds. P.M.A. Sloot et al., Lecture Notes in Computer Science 2329 (Springer-Verlag) 940
Mikić, Z., Linker, J.A., Schnack, D.D., Lionello, R., Tarditi, A. 1999, Phys. of Plasmas 6(5), 2217
Nool, M. & Keppens, R. 2002, Comp. Meth. Appl. Math. 2(1), 92
Odstrčil, D. & Pizzo, V.J. 1999, J. Geophys. Res. 104, 483
Powell, K.G., Roe, P.L., Linde, T.J., Gombosi, T.I., De Zeeuw, D.L. 1999, J. Comput. Phys. 154, 284
Tóth, G. 1996, Astrophys. Lett. Commun. 34, 245
Tóth, G. 1997, J. Comput. Phys. 138, 981
Tóth, G. 2000, J. Comput. Phys. 161, 605
Tóth, G. & Odstrčil , D. 1996, J. Comput. Phys. 128, 82
Woodward, P.R. & Colella, P. 1984, J. Comput. Phys. 54, 115
Zaliznyak, Yu., Keppens, R., Goedbloed, J.P. 2003, Phys. of Plasmas 10(11), 4478